Light-nuclei production in Au + Au collisions at $\sqrt{s_{NN}} = 3$ GeV within a thermodynamical approach: Bulk properties and collective flow

M. Kozhevnikova [1,*] and Yu. B. Ivanov [2,3,†]

[1] *Veksler and Baldin Laboratory of High Energy Physics, JINR Dubna, 141980 Dubna, Russia*

[2] *Bogoliubov Laboratory of Theoretical Physics, JINR Dubna, 141980 Dubna, Russia*

[3] *National Research Center "Kurchatov Institute," 123182 Moscow, Russia*

(Received 16 November 2023; accepted 8 January 2024; published 31 January 2024)

We present results of simulations of light-nuclei production in Au + Au collisions at a collision energy of $\sqrt{s_{NN}} = 3$ GeV within the updated Three-fluid Hydrodynamics-based Event Simulator Extended by UrQMD (ultrarelativistic quantum molecular dynamics) final State interactions (THESEUS). The results are compared with recent STAR data. The light-nuclei production is treated within the thermodynamical approach on an equal basis with hadrons. The only additional parameter related to the light nuclei is the energy density of late freeze-out that imitates the afterburner stage of the collision because the light nuclei do not participate in the UrQMD evolution. It is found that the late freeze-out is preferable for deuterons, tritons, and ^{3}He. Remarkably, the ^{4}He observables are better reproduced with the standard freeze-out. This suggests that the ^{4}He nuclei better survive in the afterburner stage because they are more spatially compact and tightly bound objects. This is an argument in favor of dynamical treatment of light nuclei. The simulations indicate that the collision dynamics is determined by the hadronic phase. The calculated results reveal a not perfect, but good reproduction of the data on bulk observables and directed flow. The elliptic flow turns out to be more intricate.

DOI: 10.1103/PhysRevC.109.014913

I. INTRODUCTION

During recent years the light-nuclei production has become again one of the central topics in studies of relativistic heavy-ion collisions. As predicted, an enhanced production of light nuclei is a promising signal of the critical endpoint (CEP) [1–3]. This prediction is based on enhancement of the nucleon attraction near the CEP due to a rapid increase of the correlation length [4] and slowing down the equilibration of the density fluctuations [5] in the critical region. Abundant production of light nuclei also results from formation of baryon clusters due to spinodal decomposition associated with a mechanically unstable region in the first-order phase transition [6–11]. These expectations have revived interest in the study of light-nuclei production at high collision energies. At lower energies, a noticeable part of the baryon charge is emitted in the form of light nuclei. Therefore, even the proton data cannot be described without proper reproduction of the light-nuclei yield. There are different approaches to light-nuclei production, which are still actively debated [12–15].

Coalescence is the most popular approach (see, e.g., Refs. [16–26]), which, however, needs additional parameters for description of the light-nuclei yield. The recently developed transport models [27–34] treat light nuclei microscopically on an equal basis with other hadrons. However, these transport models also require an extensive additional input for the light-nuclei description.

The thermodynamical approach does not need any additional parameters for the light-nuclei treatment. It describes the light nuclei on an equal basis with hadrons, i.e., in terms of temperatures and chemical potentials. This approach was first realized within the statistical model, which fairly well described deuteron midrapidity yields [35,36] at the energies from 7.7 to 200 GeV [37,38] while overestimating the tritium yield by roughly a factor of 2 [38,39]. The statistical model gave a good description of even hypernuclei and antinuclei [40].

Inspired by the relative success of the statistical model [37–40], we implemented the thermodynamic approach to the light-nuclei production into the updated Three-fluid Hydrodynamics-based Event Simulator Extended by UrQMD (ultrarelativistic quantum molecular dynamics) final State interactions (THESEUS) event generator [41]. In general, this approach involves no additional parameters inherent in light nuclei, which makes its predictive power the same for light nuclei and hadrons. However, because of the lack of the (posthydrodynamical) afterburner stage for the light nuclei we had to introduce a parameter of the late freeze-out for them [42]. This late freeze-out imitates the afterburner evolution. In Ref. [42] we considered Pb + Pb and Au + Au collisions in the collision energy range of $\sqrt{s_{NN}} = 6.4 - 19.6$ GeV. The updated THESEUS resulted in an imperfect but reasonable reproduction of data on bulk observables of the light nuclei, especially their functional dependence on the collision energy and the light-nucleus mass.

*kozhevnikova@jinr.ru

†yivanov@theor.jinr.ru

Data on light-nuclei production in Au + Au collisions at $\sqrt{s_{NN}} = 3$ GeV were recently published [43,44]. Apart from several blast-wave fits, these data on bulk properties of light nuclei were analyzed in coalescence-based three-dimensional simulations within the jet AA microscopic transport model (JAM) [45,46], the simulating many accelerated strongly-interacting hadrons model (SMASH) [47], and UrQMD [48], which were presented in the STAR paper [43], as well as in the JAM-based calculation [49]. Simulations were also performed within the parton-hadron-quantum-molecular-dynamics approach [31], in which the cluster formation occurs dynamically due to interactions, and the hybrid dynamical-statistical approach [50]. These models reproduce, albeit to varying degrees, experimental trends of the data. The data on the collective flow of light nuclei at 3 GeV [44] were analyzed within the coalescence-based JAM generator, presented in Ref. [44]. These JAM simulations well describe the data.

In the present paper, the treatment of our previous paper [42] is extended to Au + Au collisions at $\sqrt{s_{NN}} = 3$ GeV. We calculate bulk properties and directed and elliptic flows of protons and light nuclei (d, t, ^{3}He, and ^{4}He) within the updated THESEUS approach [41] based on thermodynamic treatment of light nuclei. In contrast to the collision energy range considered in Ref. [42], the yield of the light nuclei at 3 GeV plays a noticeable role in the total balance of the baryon charge.

TABLE I. Stable light nuclei and low-lying resonances of the ^{4}He system (from Brookhaven National Laboratory properties of nuclides [55]). J denotes the total angular momentum. The last column represents branching ratios of the decay channels, in percent. Here, p, n, and d correspond to the emission of protons, neutrons, and deuterons, respectively.

Nucleus [E (MeV)]	J	Decay modes, in %
d	1	Stable
t	1/2	Stable
^{3}He	1/2	Stable
^{4}He	0	Stable
^{4}He(20.21)	0	$p = 100$
^{4}He(21.01)	0	$n = 24$, $p = 76$
^{4}He(21.84)	2	$n = 37$, $p = 63$
^{4}He(23.33)	2	$n = 47$, $p = 53$
^{4}He(23.64)	1	$n = 45$, $p = 55$
^{4}He(24.25)	1	$n = 47$, $p = 50$, $d = 3$
^{4}He(25.28)	0	$n = 48$, $p = 52$
^{4}He(25.95)	1	$n = 48$, $p = 52$
^{4}He(27.42)	2	$n = 3$, $p = 3$, $d = 94$
^{4}He(28.31)	1	$n = 47$, $p = 48$, $d = 5$
^{4}He(28.37)	1	$n = 2$, $p = 2$, $d = 96$
^{4}He(28.39)	2	$n = 0.2$, $p = 0.2$, $d = 99.6$
^{4}He(28.64)	0	$d = 100$
^{4}He(28.67)	2	$d = 100$
^{4}He(29.89)	2	$n = 0.4$, $p = 0.4$, $d = 99.2$

II. UPDATED THESEUS

The THESEUS event generator [51,52] is based on the model of three-fluid dynamics (3FD) [18,53] complemented by the UrQMD [48] for the afterburner stage. The 3FD takes into account counterstreaming of the leading baryon-rich matter at the early stage of nuclear collisions. This nonequilibrium stage is modeled by means of two counterstreaming baryon-rich fluids. Newly produced particles, which dominantly populate the midrapidity region, are assigned to a so-called fireball fluid. These fluids are governed by a set of hydrodynamic equations coupled by friction terms, which describe the energy-momentum exchange between the fluids.

The output of the 3FD model, i.e., the freeze-out hypersurface, is recorded in terms of local flow velocities and thermodynamic quantities. The THESEUS generator transforms the 3FD output into a set of observed particles, i.e., performs the particlization. After the particlization the afterburner stage is described by UrQMD. First applications of the THESEUS generator to the description of heavy-ion collisions were demonstrated in Refs. [51,52].

In the initial version of the THESEUS generator [51,52], spectra of the so-called primordial nucleons, i.e., both observable nucleons and those bound in the light nuclei, were calculated. These spectra were intended for subsequent use in the coalescence model [18,54] for light-nuclei production. Therefore, the nucleons bound in the light nuclei should be subtracted from the primordial ones in order to obtain the observable nucleons. Such subtraction is performed in 3FD, where production of the light nuclei is calculated within the coalescence approach [18,54]. The initial version of THESEUS took temperature and chemical potential fields for hadron sampling from the hydrodynamic output of the 3FD (where the clusters are not included in the EoS) and produced both hadrons and clusters within the thermodynamical approach. This led to an overestimation of the total baryon charge in the final state containing both baryons and clusters. Therefore, a compensating correction was required. Such a correction was made in the updated version of THESEUS [41] by means of the recalculation of the baryon chemical potentials, proceeding from the local baryon number conservation in the system of hadrons extended by the light-nuclei species listed in Table I. The list of the light nuclei includes the stable nuclei [deuterons (d), tritons (t), and helium isotopes ^{3}He and ^{4}He] and low-lying ^{4}He resonances decaying into stable species [1]. The corresponding antinuclei are also included.

In the updated version of THESEUS [41], the light nuclei were included on an equal basis with other hadrons. These nuclei were sampled similarly to other hadrons, i.e., accordingly to their phase-space distribution functions. However, there is an important difference. While the hadrons pass through the UrQMD afterburner stage after the particlization, the light nuclei do not, because the UrQMD is not able to treat them. This is a definite shortcoming because the light nuclei are destroyed and again reproduced during the afterburner stage [27,28,30,32,33]. Following the recipe of Ref. [41], we imitate the afterburner for light nuclei by late freeze-out in the 3FD.

Three different equations of state (EoS's) are used in the 3FD simulations: a purely hadronic EoS [56] and two EoS's with deconfinement [57], i.e., an EoS with a first-order phase transition (1PT EoS) and one with a smooth crossover

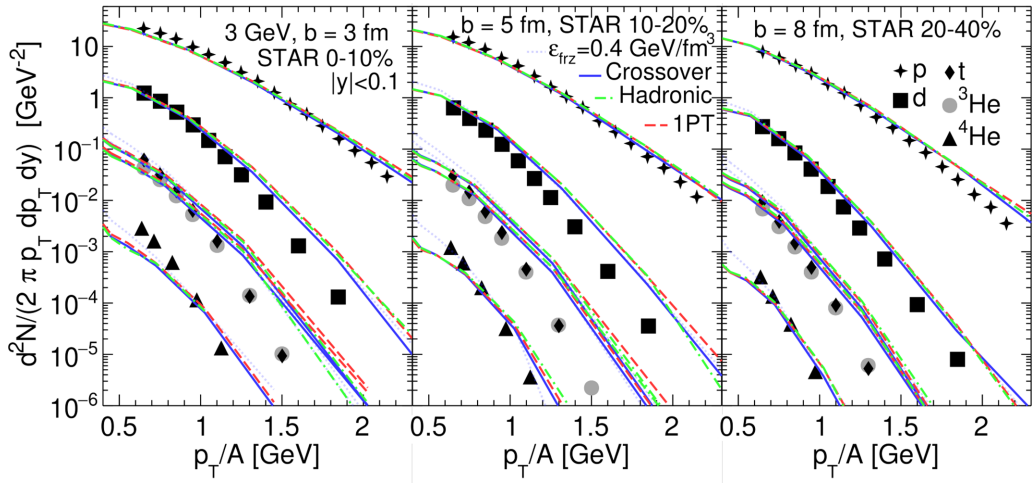

FIG. 1. Midrapidity ($|y| < 0.1$) transverse-momentum spectra of protons and light nuclei (deuterons, tritons, ^{3}He, and ^{4}He) in Au + Au collisions at a collision energy of $\sqrt{s_{NN}} = 3$ GeV and different centralities (impact parameters b). Results were calculated with hadronic, 1PT, and crossover EoS's. Results of the THESEUS simulations with the late freeze-out ($\varepsilon_{\rm frz} = 0.2\,{\rm GeV/fm^3}$) for three EoS's and the conventional 3FD freeze-out ($\varepsilon_{\rm frz} = 0.4\,{\rm GeV/fm^3}$) for the crossover EoS are displayed for light nuclei. Protons were calculated within the conventional 3FD freeze-out with the subsequent UrQMD afterburner. STAR data are from Ref. [43].

transition (crossover EoS). Consequently, the 3FD output for these EoS's is used in the THESEUS generator.

III. BULK OBSERVABLES

To partially overcome the aforementioned problem of the afterburner stage for the light nuclei, we imitate the afterburner effect by late freeze-out for light nuclei. Similarly to Ref. [41], we take the freeze-out energy density $\varepsilon_{\rm frz} = 0.2\,{\rm GeV/fm^3}$ for this late freeze-out, which looks quite suitable for all considered quantities, as seen below. No other additional tuning of the parameters was carried out for the light nuclei. Note that the conventional 3FD freeze-out energy density for all other hadrons, subjected to the UrQMD afterburner, is $0.4\,{\rm GeV/fm^3}$. Details of the freeze-out procedure in the 3FD are described in Refs. [58,59]. The $\varepsilon_{\rm frz}$ quantity has the meaning of a "trigger" that indicates the possibility of freeze-out. The freeze-out procedure begins when the local (i.e., in a cell) energy density drops below the freeze-out value $\varepsilon_{\rm frz}$, and then testing for additional freeze-out conditions starts. If all the freeze-out conditions are met, the cell is declared frozen-out. Thus, the actual energy density of a frozen-out cell turns out to be lower than $\varepsilon_{\rm frz}$, as it is demonstrated, e.g., in Ref. [60].

A. Transverse-momentum spectra

Midrapidity ($|y| < 0.1$) transverse-momentum spectra of protons and light nuclei (deuterons, tritons, ^{3}He, and ^{4}He) in Au + Au collisions at a collision energy of $\sqrt{s_{NN}} = 3$ GeV and different centralities (impact parameters b) are displayed in Fig. 1. The proton spectra were calculated within full THESEUS, i.e., with the standard 3FD freeze-out and the UrQMD afterburner. The spectra of light nuclei are evaluated for the late 3FD freeze-out without the afterburner stage. As seen, the results for different EoS's are almost identical, which means that the dynamics is dominated by the hadronic phase. The difference between the late freeze-out and the conventional 3FD freeze-out for the crossover EoS is mostly seen at low p_T for light nuclei. In the p_T spectra, this difference does not look dramatic. However, in rapidity distributions (Fig. 2), which were mostly determined by the low-p_T spectra, the difference is quite noticeable.

Similarly to previous results [42], the experimental p_T spectra [43] turn out to be steeper than the calculated ones. This is not only the problem of light-nuclei description. The proton spectra are also more flat than the experimental ones. This is a shortcoming of the 3FD model. The slight extra flatness of the proton spectra transforms into larger extra flatness of light-nuclei spectra.

As has been already noted in Ref. [42], the 3FD predictions overestimate the high-p_T ends of the spectra because of finiteness of the considered system. Even abundant hadronic probes become rare at high momenta. For the rare probes, treatment on the basis of the canonical ensemble is needed rather than within the grand canonical ensemble. The grand canonical ensemble results in overestimation of their yields. Of course, it is difficult to indicate how much of this overestimation is due to the grand canonical treatment, and not to the shortcomings of the model.

B. Rapidity distributions

Rapidity distributions of protons and light nuclei in Au + Au collisions at a collision energy of $\sqrt{s_{NN}} = 3$ GeV and different centralities are presented in Fig. 2. Again the proton distributions were calculated within full THESEUS, i.e., with the standard 3FD freeze-out and the UrQMD afterburner, while the light-nuclei distributions were calculated within the late 3FD freeze-out and without the afterburner stage. The light-nuclei distributions, calculated at the conventional 3FD freeze-out, are also displayed for comparison. The same value

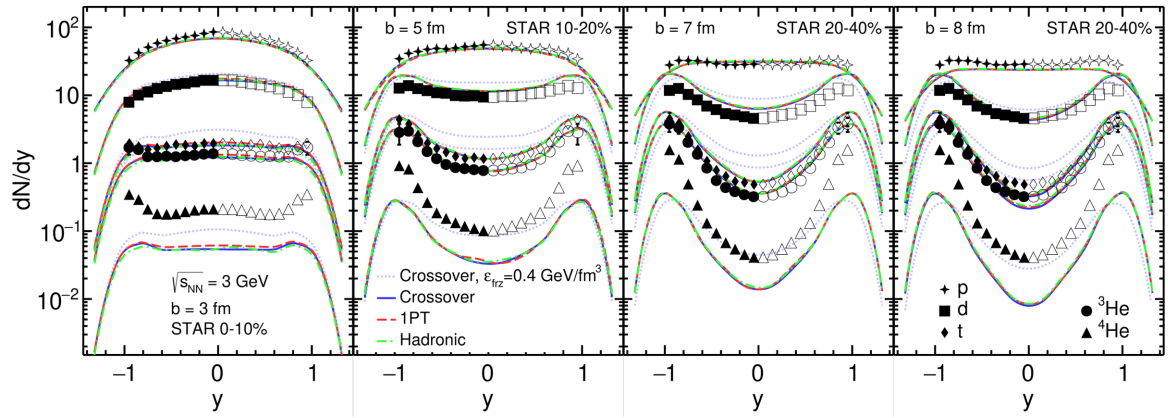

FIG. 2. Rapidity distributions of protons and light nuclei (deuterons, tritons, ^{3}He, and ^{4}He) in Au + Au collisions at a collision energy of $\sqrt{s_{NN}} = 3$ GeV and different centralities (impact parameters b). Results were calculated with hadronic, 1PT, and crossover EoS's. Results of the THESEUS simulations with the late freeze-out ($\varepsilon_{\rm frz} = 0.2\,{\rm GeV/fm^3}$) for three EoS's and the conventional 3FD freeze-out ($\varepsilon_{\rm frz} = 0.4\,{\rm GeV/fm^3}$) for the crossover EoS are displayed for light nuclei. Protons were calculated within the conventional 3FD freeze-out with the subsequent UrQMD afterburner. STAR data are from Ref. [43]. Solid symbols display measured experimental points, whereas the open ones are those reflected with respect to the midrapidity.

of the late-freeze-out energy density ($\varepsilon_{\rm frz} = 0.2\,{\rm GeV/fm^3}$) as that at higher collision energies [42] turned out to be the most suitable at 3 GeV. The reproduction of the experimental distributions turns out to be even better than that at higher collision energies [42]. The THESEUS simulations well describe the difference in the form of proton and light-nuclei distributions and its dependence on the centrality.

For the experimental centrality of 20–40% we present comparison with results for two impact parameters ($b = 7$ and 8 fm) in order to illustrate the sensitivity of the results to the choice of b. As seen, the proton rapidity density is underestimated in midrapidity at $b = 8$ fm in spite of perfect reproduction of the low-p_T experimental spectrum (see Fig. 1). The reason is that the extrapolation of the experimental spectrum to even lower p_T exceeds the THESEUS predictions. A similar situation takes place for the light nuclei. Thus, the results for two impact parameters ($b = 7$ and 8 fm) illustrate uncertainty of the THESEUS predictions.

The ^{4}He distributions deserve a separate discussion. The late-freeze-out calculation strongly underestimates these distributions. Expanding the list of light-nuclei resonances by those of ^{5}H, ^{5}He, and ^{5}Li [38], which decay into ^{4}He, makes an additional contribution to the ^{4}He yield. This additional contribution is large, i.e., of the order of 60%, in central collisions at the energy of 3 GeV, in accordance with Ref. [38]. However, it is not large enough to compensate the obtained underestimation. At the same time, the standard-freeze-out calculation results in much better (almost perfect in midrapidity at 10–20% and 20–40% centralities) reproduction of the data. The p_T spectra are also much better described by the standard freeze-out (see Fig. 1). This suggests that the ^{4}He nuclei better survive in the afterburner stage because they are more spatially compact and tightly bound objects. Then the standard freeze-out is more relevant for their description. Note that the feed-down contribution to the ^{4}He yield, ≈60% [38], is quite enough to drastically improve the reproduction midrapidity data in central collisions by the standard-freeze-out calculation.

At lower collision energies, the enhancement of the ^{4}He production is even more spectacular [61]. In central Au + Au collisions, the ^{4}He and ^{3}He yields are approximately equal at $E_{\rm lab} = 0.4A$ GeV and the ^{4}He yield even exceeds that of ^{3}He at $0.15A$ GeV. It seemingly contradicts the thermodynamic picture of the light-nuclei production. However, this contradiction is removed if the chemical freeze-out occurs earlier for ^{4}He nuclei than for d, t, and ^{3}He because of larger binding energy of the ^{4}He nuclei. In Ref. [34] it is formulated in terms of the Mott transition [62]: The observed enhancement of the ^{4}He yield can be attributed to the Mott effect on ^{4}He nuclei, which is weaker than that on deuteron, triton, and ^{3}He, as a result of its much larger binding energy. The cutoff value for the average nucleon phase-space density, $f_A^{\rm cut}$, that is used in Ref. [34], see Eq. (5) in Ref. [34], in fact plays the role of the effective freeze-out for different light nuclei. As found in Ref. [34], the $f_{A=4}^{\rm cut}$ value is approximately twice as large as that for lighter nuclei. This is consistent with our conclusion about the earlier freeze-out of ^{4}He. In particular, the results of the kinetic approach of Ref. [34] imply that the freeze-out parameters for each light-nuclei species are individual and depend on the binding energy of the considered nucleus.

C. Medium effects

Study of the in-medium effects in light-nuclei production started long ago [63]. Later, coupled quantum kinetic equations were derived that describe the time evolution of the Wigner distribution functions for nucleons and light clusters [64]. An alternative approach has also been proposed within the antisymmetrized molecular dynamics approach [65], in which nucleons are represented in terms of quantal wave packets, which are antisymmetrized with each other. These approaches have been successfully applied to analysis of results of the GANIL experiment at $50A$ MeV.

In Refs. [66,67], it was proposed to extend the study of these in-medium effects to nuclear collisions at energies available at the Nuclotron-based Ion Collider Facility and the Facility for Antiproton and Ion Research. A suitable frame for such a study is the thermodynamic approach to light-nuclei production complemented by a quantum statistical approach that includes medium effects due to Pauli blocking and self-energies [62,68,69]. This quantum statistical approach is based on the relativistic mean-field model of Ref. [68]. The energies of light nuclei are given by the formula

$$E_A(\mathbf{p}) = E_A^0(\mathbf{p}) + \Delta E_A^{\mathrm{SE}}(\mathbf{p}) + \Delta E_A^{\mathrm{Pauli}}(\mathbf{p}), \qquad (1)$$

where $E_A^0(p)$ is the vacuum energy of the A nucleus with momentum $\mathbf{p}$, $\Delta E_A^{\mathrm{SE}}(p)$ is the in-medium self-energy shift, and $\Delta E_A^{\mathrm{Pauli}}(p)$ is the energy correction due to the Pauli blocking. The last two quantities also depend on the baryon density, the temperature, and the proton/neutron asymmetry of the matter. More details can be found in Ref. [69]. This quantum statistical approach was incorporated into THESEUS at the particlization stage.

Preliminary results showed [70,71] that the best description of the light-nuclei yields is obtained when the self-energy effects are discarded at few-GeV collision energies ($\sqrt{s_{NN}}$). However, those results were not conclusive because the proper conservation of the baryon charge was not achieved in that version of THESEUS (see Sec. II). The Pauli-blocking effects were disregarded in those calculations.

The present calculation are performed within the updated version of THESEUS, where the conservation of the baryon charge is strictly fulfilled. An upper estimate of the Pauli-blocking effect is also made by means of its approximation by that at zero light-nucleus momentum in the rest frame the medium. The Pauli-blocking is strongest at this zero momentum. The Pauli-blocking effect turned out to be negligibly small because of high freeze-out temperatures as compared with the corresponding Fermi energies. The results of this calculation with the crossover EoS are displayed in Fig. 3. As seen, the medium effect accordingly to Ref. [69] turns out to be too strong. It results in strong disagreement with the data, as has been already seen from the preliminary simulations [70,71]. Even the proton yield is overestimated. Apparently this is because the relativistic mean-field model [68], underlying these medium corrections, has been parametrized to reproduce low-energy nuclear phenomena. This parametrization is simply inapplicable to highly excited nuclear matter. Of course, we could introduce a temperature-dependent attenuation factor to reduce the strength of these medium corrections. However, it would be a purely phenomenological tuning parameter. Therefore, we avoid doing this.

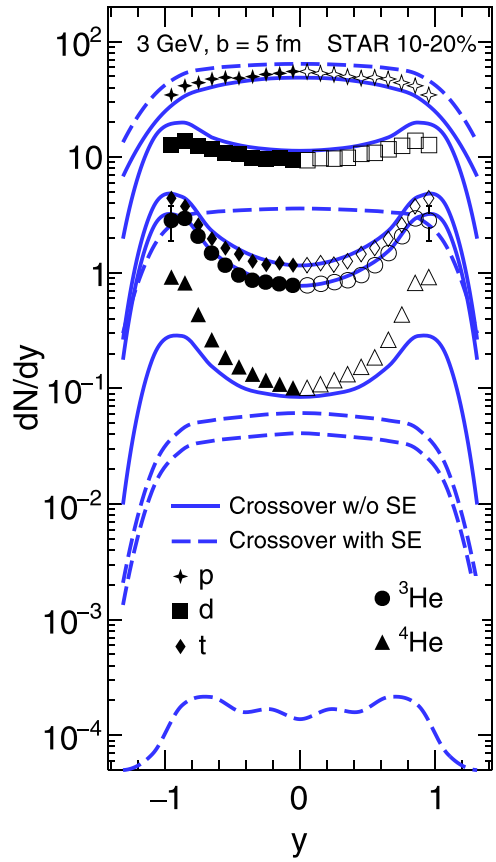

FIG. 3. Rapidity distributions of protons and light nuclei (from the top down: protons, deuterons, tritons, ^{3}He, and ^{4}He) in Au + Au collisions at a collision energy of $\sqrt{s_{NN}} = 3$ GeV and $b = 5$ fm. Results were calculated in the crossover scenario with (with SE) and without (w/o SE) the self-energy contributions, i.e., the $\Delta E_A^{\mathrm{SE}}(\mathbf{p})$ and $\Delta E_A^{\mathrm{Pauli}}(\mathbf{p})$ terms in Eq. (1). Protons were calculated within the conventional 3FD freeze-out with the subsequent UrQMD afterburner. Deuterons, tritons, and ^{3}He were calculated with the late freeze-out ($\varepsilon_{\mathrm{frz}} = 0.2\,\mathrm{GeV/fm^3}$), while ^{4}He is calculated with the conventional 3FD freeze-out ($\varepsilon_{\mathrm{frz}} = 0.4\,\mathrm{GeV/fm^3}$). STAR data are from Ref. [43]. Solid symbols display measured experimental points, whereas the open ones are those reflected with respect to the midrapidity.

IV. COLLECTIVE FLOW

Collective flow is a more subtle observable of the heavy-ion collisions. Its calculation with the thermodynamic approach is straightforward because light nuclei are treated on an equal basis with other hadrons. Results for the collective flow, which are presented below, are calculated with respect to the reaction plane that is exactly defined in the simulations. We have also done calculations with the event plane determined after the afterburner in terms of observable particles within the STAR acceptance. The reaction-plane and event-plane results turned out to be practically identical.

A. Directed flow

The calculated directed flow of protons and light nuclei (deuterons, ^{3}He, and ^{4}He) as a function of rapidity in semi-central ($b = 6$ fm) Au + Au collisions at a collision energy of $\sqrt{s_{NN}} = 3$ GeV is presented in Fig. 4. The results are compared with STAR data [44,72]. We do not display results for the tritons because they are very similar to those for ^{3}He, including the degree of agreement with the data. The THESEUS simulations for light nuclei were performed for the late freeze-out ($\varepsilon_{\mathrm{frz}} = 0.2\,\mathrm{GeV/fm^3}$) for three EoS's. Protons were calculated within the conventional 3FD freeze-out with the subsequent UrQMD afterburner.

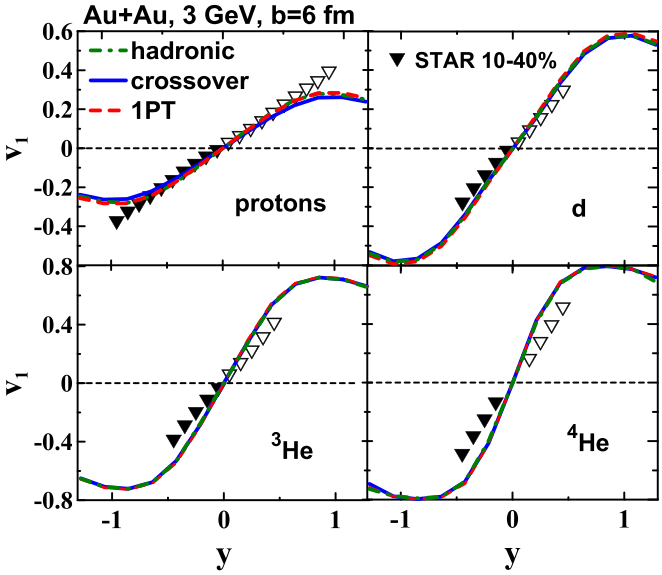

FIG. 4. Directed flow of protons and light nuclei (deuterons, ^{3}He, and ^{4}He) as a function of rapidity in semicentral ($b = 6$ fm) Au + Au collisions at a collision energy of $\sqrt{s_{NN}} = 3$ GeV. Results were calculated with hadronic, 1PT, and crossover EoS's. Results of the THESEUS simulations with the late freeze-out ($\varepsilon_{\rm frz} = 0.2\,{\rm GeV/fm^3}$) are displayed for light nuclei. Protons were calculated within the conventional 3FD freeze-out with the subsequent UrQMD afterburner. STAR data are from Refs. [44,72]. Solid symbols display measured experimental points, whereas the open ones are those reflected with respect to the midrapidity.

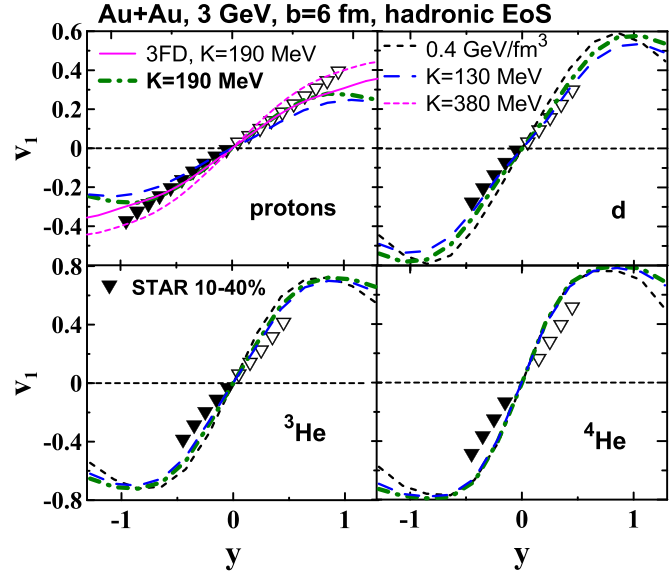

FIG. 5. The same as in Fig. 4 but for various versions of hadronic EoS: the standard hadronic EoS ($K = 190$ MeV) and very soft hadronic EoS ($K = 130$ MeV). Results of the THESEUS simulations with the late freeze-out ($\varepsilon_{\rm frz} = 0.2\,{\rm GeV/fm^3}$) and conventional 3FD freeze-out ($\varepsilon_{\rm frz} = 0.4\,{\rm GeV/fm^3}$) are displayed for light nuclei. Protons were calculated within the conventional 3FD freeze-out with the subsequent UrQMD afterburner. The proton v_1 within the 3FD model, i.e., before the UrQMD afterburner, is also presented for the standard EoS ($K = 190$ MeV, thin solid line) and the stiff EoS ($K = 380$ MeV, thin short-dashed line).

The directed flow turns out to be independent of the used EoS, which again suggests that the dynamics is dominated by the hadronic phase. The calculated results almost perfectly (except for very forward and backward rapidities) reproduce the experimental proton directed flow [72]. Agreement with the data [44] is getting worse with increase of the atomic number of the light nucleus. If the calculated midrapidity slope of the directed flow is only slightly steeper than the experimental one for deuterons, for ^{4}He it is already noticeably steeper.

To check if this disagreement is related to the above-observed preference of the conventional freeze-out for ^{4}He (see Fig. 2), we present the results with conventional 3FD freeze-out in Fig. 5. As seen, the ^{4}He flow is independent of the type of the freeze-out, while the flow slopes of lighter nuclei become only slightly steeper at the conventional freeze-out.

Stiffness of the hadronic EoS with the 3FD model can be easily changed. The stiffness is characterized by incompressibility of nuclear matter that is conventionally defined as

$$K = 9n_0^2 \frac{d^2}{dn^2}\left(\frac{\varepsilon(n, T=0)}{n}\right)_{n=n_0}, \qquad (2)$$

where $\varepsilon(n, T = 0)$ is the energy density of the nuclear matter at zero temperature ($T = 0$) as a function of the baryon density (n), and n_0 is the normal nuclear density. The conventionally used hadronic EoS is characterized by $K = 190$ MeV. This is a quite soft EoS. It is very similar (but not identical) to the EoS of the hadronic phase in the 1PT and crossover EoS's [57]. To study the effect of the EoS stiffness on the directed flow, we present results for a very soft hadronic EoS ($K = 130$ MeV) in Fig. 5. As seen, the ^{4}He flow again turns out to be independent of the EoS stiffness. The very soft EoS gives slightly better agreement with the data for lighter nuclei than the conventionally used EoS but results in disagreement with the experimental proton flow. In Ref. [72] it is reported that the stiff hadronic EoS ($K = 380$ MeV) well reproduces the proton directed flow within the UrQMD and JAM models. In contrast, our calculation shows that the stiff EoS ($K = 380$ MeV) results in a too steep slope of the proton flow (see the thin short-dashed line in Fig. 5), which leads to even stronger disagreement with flow data for light nuclei. Therefore, the conventionally used soft hadronic EoS with $K = 190$ MeV seems to be the optimal choice. This conclusion agrees with Ref. [73], published more than 20 years ago.

The proton v_1 within the 3FD model, i.e., before the UrQMD afterburner, is also presented in Fig. 5. The afterburner does not change the midrapidity slope of the flow but worsens agreement with the data at very forward and backward rapidities. The proton flow at the late freeze-out and without afterburner (not displayed in Fig. 5) is very similar to that at the conventional 3FD freeze-out and the subsequent afterburner, which once again confirms the correctness of the choice of energy density for the late freeze-out.

In contrast to the proton flow, the afterburner imitation (i.e., the late freeze-out) does change the midrapidity slope

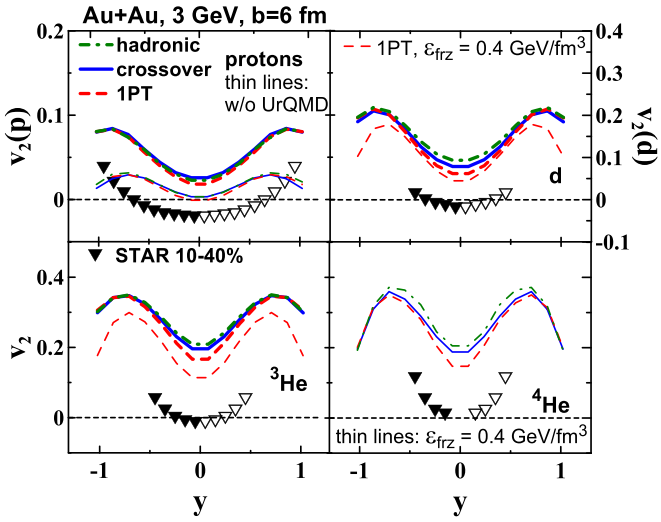

FIG. 6. Elliptic flow of protons and light nuclei (deuterons, ^{3}He, and ^{4}He) as a function of rapidity in semicentral ($b = 6$ fm) Au + Au collisions at a collision energy of $\sqrt{s_{NN}} = 3$ GeV. Results were calculated with hadronic, 1PT, and crossover EoS's. Results of the THESEUS simulations with three EoS's are displayed for deuterons and ^{3}He at the late freeze-out ($\varepsilon_{\rm frz} = 0.2\,{\rm GeV/fm^3}$) and for the ^{4}He nuclei at the conventional 3FD freeze-out ($\varepsilon_{\rm frz} = 0.4\,{\rm GeV/fm^3}$). The conventional 3FD freeze-out with the 1PT EoS is also presented for deuterons and ^{3}He. Protons were calculated within the conventional 3FD freeze-out with the subsequent UrQMD afterburner. The proton v_2 flows before the UrQMD afterburner are also presented. STAR data are from Refs. [44,72]. Solid symbols display measured experimental points, whereas the open ones are those reflected with respect to the midrapidity.

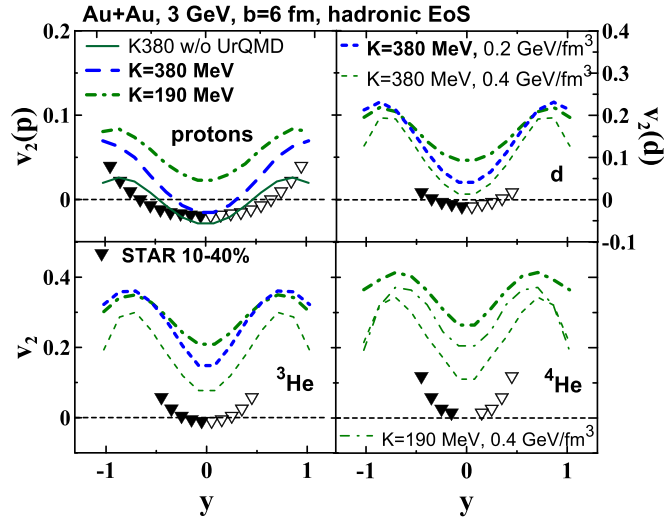

FIG. 7. The same as in Fig. 6 but for various versions of the hadronic EoS. Results with the standard hadronic EoS ($K = 190$ MeV) are displayed by bold dash-dotted lines for the late freeze-out ($\varepsilon_{\rm frz} = 0.2\,{\rm GeV/fm^3}$) for all light nuclei and by a thin dash-dotted line for the standard 3FD freeze-out ($\varepsilon_{\rm frz} = 0.4\,{\rm GeV/fm^3}$) for ^{4}He nuclei. Results of calculations with the stiff hadronic EoS ($K = 380$ MeV) are also presented: for deuterons and ^{3}He at the late freeze-out and for all nuclei at the standard 3FD freeze-out. Protons were calculated within the conventional 3FD freeze-out with the subsequent UrQMD afterburner. The proton v_2 before the UrQMD afterburner is also presented for the stiff EoS ($K = 380$ MeV) by a solid line.

of deuterons and ^{3}He albeit slightly. However, the ^{4}He flow is not affected by the late freeze-out.

B. Elliptic flow

The calculated elliptic flow of protons and light nuclei (deuterons, ^{3}He, and ^{4}He) as a function of rapidity in semicentral ($b = 6$ fm) Au + Au collisions at a collision energy of $\sqrt{s_{NN}} = 3$ GeV is presented in Fig. 6. The results are compared with STAR data [44,72]. Results for tritons are again omitted because they are very similar to those for ^{3}He. The THESEUS simulations for deuterons and ^{3}He were performed for the late freeze-out ($\varepsilon_{\rm frz} = 0.2\,{\rm GeV/fm^3}$), while for ^{4}He, the conventional 3FD freeze-out ($\varepsilon_{\rm frz} = 0.4\,{\rm GeV/fm^3}$) was used in view of its preference for p_T spectra and y distributions (see Sec. III). Protons were calculated within the conventional 3FD freeze-out with the subsequent UrQMD afterburner. For comparison, the light-nuclei flow with the conventional 3FD freeze-out for the 1PT EoS and the proton v_2 flow before the UrQMD afterburner are also demonstrated.

As seen from Fig. 6, the calculated elliptic flow considerably overestimates the data [44,72]. Even the v_2 sign is different in the midrapidity region. The afterburner (for protons) and the late freeze-out (for light nuclei) even worsen agreement with the data. The large disagreement of light-nuclei elliptic flow with the data [44] does not mean that the thermodynamic approach fails to describe this flow. This only means that the 3FD model has trouble describing the elliptic flow of protons, which transforms into even bigger trouble for light nuclei.

As stated in Refs. [44,72,73], a stiff EoS is needed for describing the elliptic flow. Therefore, we performed simulations with a stiff hadronic EoS ($K = 380$ MeV) (see Fig. 7). The results became closer to the data. The proton elliptic flow was even reproduced in the midrapidity. However, the overall disagreement with data remains. The afterburner (late freeze-out) still worsens the agreement with the data.

Note that dips and even negative values of v_2 in the midrapidity are consequences of the squeeze-out effect [74–76], which result from blocking of the expanding central blob by the spectator matter. The squeeze-out is a characteristic feature of moderately relativistic collisions, in which the expanding central fireball is shadowed by spectators. This shadowing only partially is taken into account within the 3FD evolution because the frozen-out matter of the central fireball remains to be shadowed even after the freeze-out, while in the 3FD model it escapes without interacting with spectators. The afterburning stage should, in principle, correct this deficiency. However, it does not, as we see from Figs. 7 and 6. The reason is that the THESEUS generator assigns *the same time instant* to all produced particles during the particlization procedure, while different parts of the system are frozen-out at *different time instants* in 3FD. Participants are frozen-out earlier than spectators. If the particlization is isochronous, the evolution

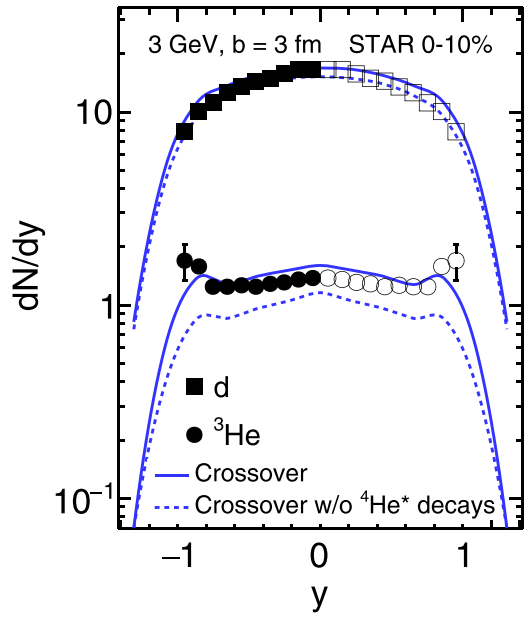

FIG. 8. Rapidity distributions of light nuclei (deuterons and ^{3}He) in central Au + Au collisions at collision energy of $\sqrt{s_{NN}} = 3$ GeV. Results were calculated in the crossover scenario with and without (w/o ^{4}He* decays) the feed-down contributions. STAR data are from Ref. [43]. Solid symbols display measured experimental points, whereas the open ones are those reflected with respect to the midrapidity.

of the frozen-out participants stops until the spectators also become frozen-out. Therefore, we skip the stage of shading the afterburner expansion of the central fireball by spectators still being in the hydrodynamic phase. The afterburner evolution is switched on only when the spectators also become frozen-out. The spectators are frozen-out when they have already passed the expanding central fireball. Thus, the shadowing by spectators turns out to be strongly reduced after such isochronous particlization compared to what it would be if the entire collision process were kinetically treated, as in UrQMD or JAM. Apparently, this is the prime reason of failure of the elliptic-flow description. A time-extended transition from hydrodynamic evolution to afterburner dynamics would need to take into account the interaction of the kinetic afterburner phase with still hydrodynamically evolved matter. This is a difficult task both technically and conceptually.

V. FEED-DOWN FROM UNSTABLE ^{4}He

As found in Ref. [42], the feed-down contributions from unstable ^{4}He to deuterons are negligibly small, while to tritons and ^{3}He the feed-down contributions are less than 20% at $\sqrt{s_{NN}} > 6$ GeV in the midrapidity. At the forward/backward rapidities, these contributions are essential even at $\sqrt{s_{NN}} > 6$ GeV. It has been predicted [38] that feed-down contributions reach values of the order of 60% for tritons and ^{3}He even in midrapidity at $\sqrt{s_{NN}} = 3$ GeV.

Results of our calculations are presented in Fig. 8 in the example of the crossover EoS. In agreement with Ref. [38], the feed-down contribution amounts to ∼20% for deuterons and 50–100% (depending on the rapidity) for ^{3}He. While the feed-down contribution into the deuteron yield is inessential for the data reproduction, it plays an important role for ^{3}He. Without this feed-down the ^{3}He yield is noticeably underestimated.

The v_1 flow of deuterons, tritons, and ^{3}He turns out to be insensitive to the feed-down contributions from unstable ^{4}He. Without these contributions, the corresponding v_2 flows are reduced by ∼20%, which, however, does not essentially change the degree of their agreement with the data. The effect on the proton yield and flow is negligible.

VI. SUMMARY

Simulations of the proton and light-nuclei production in Au + Au collisions at $\sqrt{s_{NN}} = 3$ GeV were performed within the updated THESEUS event generator [41]. The results were compared with recent STAR data [43,44]. The updated THESEUS treats the light-nuclei production within the thermodynamical approach on an equal basis with hadrons. The protons (as well as other hadrons) are calculated with the standard 3FD freeze-out, characterized by the energy density of $\varepsilon_{\rm frz} = 0.4\,{\rm GeV/fm}^3$, followed by the UrQMD afterburner. The only additional parameter related to the light nuclei is the energy density of the late freeze-out that imitates the afterburner stage because the light nuclei do not participate in the UrQMD evolution.

In fact, the freeze-out parameter is required in both the thermodynamical approach and the coalescence approach. Both approaches are inapplicable at very early freeze-out, when interparticle spacing in a fireball is less than the internucleon distance in a light nucleus. At later freeze-out, the light-nuclei yields crucially depend on the freeze-out conditions in both approaches. The coalescence allows fine-tuning of the light-nuclei production after the freeze-out by means of coalescence parameters. In contrast, within the thermodynamical approach, the light-nuclei observables are solely determined by the applied freeze-out in the absence of the afterburner. Dynamical treatment of the light nuclei at the afterburner stage [27,28,32,33] would essentially weaken this strong dependence on the freeze-out.

It was found that the late freeze-out characterized by $\varepsilon_{\rm late\ frz} = 0.2\,{\rm GeV/fm}^3$ is preferable for deuterons, tritons, and ^{3}He. This is precisely the same value of $\varepsilon_{\rm late\ frz}$ that was found in Ref. [42] at higher collision energies. Remarkably, the ^{4}He yield and p_T spectra are better reproduced with the standard 3FD freeze-out. This suggests that the ^{4}He nuclei better survive in the afterburner stage because they are more spatially compact and tightly bound objects. This is an argument in favor of dynamical treatment of light nuclei.

Results of simulations with different EoS's (with and without transition to the quark-gluon phase) indicated that the dynamics is determined by the hadronic phase. The calculated results revealed a not perfect, but good reproduction of the data on bulk observables of the light nuclei. The calculated proton directed flow almost perfectly (except for very forward and backward rapidities) reproduces the experimental flow [72]. Agreement with the data on the directed flow [44] becomes worse with increase of the atomic number of the light

nucleus. If the calculated midrapidity slope of the directed flow is only slightly steeper than the experimental one for deuterons, for ^{4}He it is already noticeably steeper.

The model failed to properly describe the data on the elliptic flow of both protons and light nuclei. We attribute this to shortcomings of the transition from the 3FD evolution to the UrQMD afterburner, which prevents us from proper description of the squeeze-out effect. The squeeze-out results from shadowing of the expanding central fireball by spectators. This shadowing is only partially taken into account within the 3FD evolution because the frozen-out matter of the central fireball remains to be shadowed even after the freeze-out, while in the 3FD model it escapes without interacting with spectators. The afterburning stage should, in principle, correct this deficiency, but it does not. The reason is that the THESEUS generator assigns the same time instant to all produced particles during the particlization procedure, while different parts of the system get frozen-out at different time instants in 3FD. The shadowing by spectators is strongly reduced after such isochronous particlization because the participants and spectators turn out to be well separated in the thus constructed pre-afterburner configuration.

We also studied the feed-down contributions from unstable ^{4}He and possible in-medium effects. As found, the feed-down contribution amounts to ∼20% for deuterons and 50–100% (depending on the rapidity) for tritium and ^{3}He. While the feed-down contribution into the deuteron yield is inessential for the data reproduction, it plays an important role for tritium and ^{3}He. Without this feed-down the tritium and ^{3}He yields are noticeably underestimated. The medium effect accordingly to Ref. [69] turned out to be too strong and resulted in strong disagreement with the data. Apparently this is because the relativistic mean-field model [68], underlying these medium corrections, has been parametrized to reproduce low-energy nuclear phenomena. This parametrization is simply inapplicable to highly excited nuclear matter.

Development of a new hybrid model called MUFFIN (MUlti Fluid simulation for Fast IoN collisions) was recently announced in Ref. [77]. This is a next-generation hybrid three-fluid model for simulating heavy-ion collisions at energies from few to few tens of GeV. Several methodical and conceptual improvements, as compared with THESEUS, are introduced in MUFFIN. An important conceptual improvement is the inclusion of initial state fluctuations, which are important when considering the collective flow and allow study of fluctuations associated with the CEP. The afterburner based on SMASH will make it possible to describe the afterburner evolution of at least deuterons. This could resolve some of the aforementioned problems in THESEUS.

ACKNOWLEDGMENTS

We are sincerely grateful to Iurii Karpenko and David Blaschke who made enormous contributions early on in the implementation of this project. Fruitful discussions with D. N. Voskresensky are gratefully acknowledged. This work was carried out using computing resources of the federal collective usage center "Complex for simulation and data processing for mega-science facilities" at NRC "Kurchatov Institute" [78] and computing resources of the supercomputer "Govorun" at JINR [79].

[1] E. Shuryak and J. M. Torres-Rincon, Baryon preclustering at the freeze-out of heavy-ion collisions and light-nuclei production, Phys. Rev. C **101**, 034914 (2020).
[2] E. Shuryak and J. M. Torres-Rincon, Light-nuclei production and search for the QCD critical point, Eur. Phys. J. A **56**, 241 (2020).
[3] K. J. Sun, F. Li, and C. M. Ko, Effects of QCD critical point on light nuclei production, Phys. Lett. B **816**, 136258 (2021).
[4] M. A. Stephanov, K. Rajagopal, and E. V. Shuryak, Signatures of the tricritical point in QCD, Phys. Rev. Lett. **81**, 4816 (1998).
[5] B. Berdnikov and K. Rajagopal, Slowing out-of-equilibrium near the QCD critical point, Phys. Rev. D **61**, 105017 (2000).
[6] V. V. Skokov and D. N. Voskresensky, Hydrodynamical description of a hadron-quark first-order phase transition, JETP Lett. **90**, 223 (2009).
[7] V. V. Skokov and D. N. Voskresensky, Hydrodynamical description of first-order phase transitions: Analytical treatment and numerical modeling, Nucl. Phys. A **828**, 401 (2009).
[8] J. Randrup, Phase transition dynamics for baryon-dense matter, Phys. Rev. C **79**, 054911 (2009).
[9] J. Steinheimer and J. Randrup, Spinodal amplification of density fluctuations in fluid-dynamical simulations of relativistic nuclear collisions, Phys. Rev. Lett. **109**, 212301 (2012).
[10] J. Steinheimer, L. Pang, K. Zhou, V. Koch, J. Randrup, and H. Stoecker, A machine learning study to identify spinodal clumping in high energy nuclear collisions, J. High Energy Phys. 12 (2019) 122.
[11] K. J. Sun, W. H. Zhou, L. W. Chen, C. M. Ko, F. Li, R. Wang, and J. Xu, Spinodal enhancement of light nuclei yield ratio in relativistic heavy ion collisions, arXiv:2205.11010.
[12] S. Mrowczynski, Production of light nuclei at colliders—coalescence vs. thermal model, Eur. Phys. J.: Spec. Top. **229**, 3559 (2020).
[13] A. Motornenko, J. Steinheimer, V. Vovchenko, R. Stock, and H. Stoecker, Ambiguities in the hadro-chemical freeze-out of Au + Au collisions at SIS18 energies and how to resolve them, Phys. Lett. B **822**, 136703 (2021).
[14] A. Kittiratpattana, T. Reichert, P. Li, A. Limphirat, C. Herold, J. Steinheimer, and M. Bleicher, Investigating the cluster production mechanism with isospin triggering: Thermal models versus coalescence models, Phys. Rev. C **107**, 044911 (2023).
[15] V. Kireyeu, G. Coci, S. Glaessel, J. Aichelin, C. Blume, and E. Bratkovskaya, Cluster formation near midrapidity—can the mechanism be identified experimentally?, arXiv:2304.12019.
[16] J. Aichelin, "Quantum" molecular dynamics—A Dynamical microscopic *n*-body approach to investigate fragment formation and the nuclear equation of state in heavy ion collisions, Phys. Rep. **202**, 233 (1991).
[17] V. N. Russkikh, Y. B. Ivanov, Y. E. Pokrovsky, and P. A. Henning, Analysis of intermediate-energy heavy-ion collisions

within relativistic-mean field two-fluid model, Nucl. Phys. A **572**, 749 (1994).
[18] Y. B. Ivanov, V. N. Russkikh and V. D. Toneev, Relativistic heavy-ion collisions within three-fluid hydrodynamics: Hadronic scenario, Phys. Rev. C **73**, 044904 (2006).
[19] H. Liu, D. Zhang, S. He, K. J. Sun, N. Yu, and X. Luo, Light nuclei production in Au + Au collisions at $\sqrt{s_{\rm NN}} = 5-200$ GeV from JAM model, Phys. Lett. B **805**, 135452 (2020).
[20] L. Zhu, C. M. Ko, and X. Yin, Light (anti-)nuclei production and flow in relativistic heavy-ion collisions, Phys. Rev. C **92**, 064911 (2015).
[21] J. Steinheimer, K. Gudima, A. Botvina, I. Mishustin, M. Bleicher, and H. Stocker, Hypernuclei, dibaryon and antinuclei production in high energy heavy ion collisions: Thermal production vs. coalescence, Phys. Lett. B **714**, 85 (2012).
[22] Z. J. Dong, G. Chen, Q. Y. Wang, Z. L. She, Y. L. Yan, F. X. Liu, D. M. Zhou, and B. H. Sa, Energy dependence of light (anti)nuclei and (anti)hypertriton production in the Au-Au collision from $\sqrt{s_{NN}} = 11.5$ to 5020 GeV, Eur. Phys. J. A **54**, 144 (2018).
[23] S. Sombun, K. Tomuang, A. Limphirat, P. Hillmann, C. Herold, J. Steinheimer, Y. Yan, and M. Bleicher, Deuteron production from phase-space coalescence in the UrQMD approach, Phys. Rev. C **99**, 014901 (2019).
[24] P. Hillmann, K. Käfer, J. Steinheimer, V. Vovchenko, and M. Bleicher, Coalescence, the thermal model and multifragmentation: The energy and volume dependence of light nuclei production in heavy ion collisions, J. Phys. G: Nucl. Part. Phys. **49**, 055107 (2022).
[25] W. Zhao, C. Shen, C. M. Ko, Q. Liu, and H. Song, Beam-energy dependence of the production of light nuclei in Au + Au collisions, Phys. Rev. C **102**, 044912 (2020).
[26] W. Zhao, K. J. Sun, C. M. Ko, and X. Luo, Multiplicity scaling of light nuclei production in relativistic heavy-ion collisions, Phys. Lett. B **820**, 136571 (2021).
[27] D. Oliinychenko, L. G. Pang, H. Elfner, and V. Koch, Microscopic study of deuteron production in PbPb collisions at $\sqrt{s} = 2.76$ TeV via hydrodynamics and a hadronic afterburner, Phys. Rev. C **99**, 044907 (2019).
[28] J. Staudenmaier, D. Oliinychenko, J. M. Torres-Rincon, and H. Elfner, Deuteron production in relativistic heavy ion collisions via stochastic multiparticle reactions, Phys. Rev. C **104**, 034908 (2021).
[29] J. Aichelin, E. Bratkovskaya, A. Le Fèvre, V. Kireyeu, V. Kolesnikov, Y. Leifels, V. Voronyuk, and G. Coci, Parton-hadron-quantum-molecular dynamics: A novel microscopic *n*-body transport approach for heavy-ion collisions, dynamical cluster formation, and hypernuclei production, Phys. Rev. C **101**, 044905 (2020).
[30] S. Gläßel, V. Kireyeu, V. Voronyuk, J. Aichelin, C. Blume, E. Bratkovskaya, G. Coci, V. Kolesnikov, and M. Winn, Cluster and hypercluster production in relativistic heavy-ion collisions within the parton-hadron-quantum-molecular-dynamics approach, Phys. Rev. C **105**, 014908 (2022).
[31] E. Bratkovskaya, S. Glässel, V. Kireyeu, J. Aichelin, M. Bleicher, C. Blume, G. Coci, V. Kolesnikov, J. Steinheimer, and V. Voronyuk, Midrapidity cluster formation in heavy-ion collisions, EPJ Web Conf. **276**, 03005 (2023).
[32] K. J. Sun, R. Wang, C. M. Ko, Y. G. Ma, and C. Shen, Relativistic kinetic approach to light nuclei production in high-energy nuclear collisions, arXiv:2106.12742.
[33] K. J. Sun, R. Wang, C. M. Ko, Y. G. Ma, and C. Shen, Unveiling the dynamics of nucleosynthesis in relativistic heavy-ion collisions, arXiv:2207.12532.
[34] R. Wang, Y. G. Ma, L. W. Chen, C. M. Ko, K. J. Sun, and Z. Zhang, Kinetic approach of light-nuclei production in intermediate-energy heavy-ion collisions, Phys. Rev. C **108**, L031601 (2023).
[35] J. Adam *et al.* (STAR Collaboration), Beam energy dependence of (anti-)deuteron production in Au + Au collisions at the BNL Relativistic Heavy Ion Collider, Phys. Rev. C **99**, 064905 (2019).
[36] M. I. Abdulhamid *et al.* (STAR Collaboration), Beam energy dependence of triton production and yield ratio ($N_t \times N_p/N_d^2$) in Au + Au collisions at RHIC, Phys. Rev. Lett. **130**, 202301 (2023).
[37] A. Andronic, P. Braun-Munzinger, J. Stachel, and H. Stocker, Production of light nuclei, hypernuclei and their antiparticles in relativistic nuclear collisions, Phys. Lett. B **697**, 203 (2011).
[38] V. Vovchenko, B. Dönigus, B. Kardan, M. Lorenz, and H. Stoecker, Feeddown contributions from unstable nuclei in relativistic heavy-ion collisions, Phys. Lett. B **809**, 135746 (2020).
[39] D. Zhang (STAR Collaboration), Light nuclei (d, t) Production in Au + Au Collisions at $\sqrt{s_{NN}} = 7.7-200$ GeV, Nucl. Phys. A **1005**, 121825 (2021); Energy dependence of light nuclei (d, t) production at STAR, JPS Conf. Proc. **32**, 010069 (2020).
[40] A. Andronic, P. Braun-Munzinger, K. Redlich, and J. Stachel, Decoding the phase structure of QCD via particle production at high energy, Nature (London) **561**, 321 (2018).
[41] M. Kozhevnikova, Y. B. Ivanov, I. Karpenko, D. Blaschke, and O. Rogachevsky, Update of the three-fluid hydrodynamics-based event simulator: Light-nuclei production in heavy-ion collisions, Phys. Rev. C **103**, 044905 (2021).
[42] M. Kozhevnikova and Y. B. Ivanov, Light-nuclei production in heavy-ion collisions within a thermodynamical approach, Phys. Rev. C **107**, 024903 (2023); Light-nuclei production in heavy-ion collisions at $\sqrt{s_{NN}} = 6.4$–19.6 GeV in THESEUS generator based on three-fluid dynamics, Particles **6**, 440 (2023).
[43] STAR Collaboration, Production of protons and light nuclei in Au + Au collisions at $\sqrt{s_{\rm NN}} = 3$ GeV with the STAR detector, arXiv:2311.11020.
[44] M. S. Abdallah *et al.* (STAR Collaboration), Light nuclei collectivity from $\sqrt{s_{NN}} = 3$ GeV Au + Au collisions at RHIC, Phys. Lett. B **827**, 136941 (2022).
[45] Y. Nara, N. Otuka, A. Ohnishi, K. Niita, and S. Chiba, Relativistic nuclear collisions at 10*A* GeV energies from p + Be to Au + Au with the hadronic cascade model, Phys. Rev. C **61**, 024901 (1999).
[46] M. Isse, A. Ohnishi, N. Otuka, P. K. Sahu, and Y. Nara, Mean-field effects on collective flows in high-energy heavy-ion collisions from AGS to SPS energies, Phys. Rev. C **72**, 064908 (2005).
[47] J. Weil *et al.* (SMASH Collaboration), Particle production and equilibrium properties within a new hadron transport approach for heavy-ion collisions, Phys. Rev. C **94**, 054905 (2016).
[48] S. A. Bass, M. Belkacem, M. Bleicher, M. Brandstetter, L. Bravina, C. Ernst, L. Gerland, M. Hofmann, S. Hofmann, J. Konopka *et al.*, Microscopic models for ultrarelativistic heavy ion collisions, Prog. Part. Nucl. Phys. **41**, 255 (1998).
[49] Y. Xu, X. He, and N. Xu, Light nuclei production in Au + Au collisions at 3 GeV from coalescence model, Chin. Phys. C **47**, 074107 (2023).

[50] N. Buyukcizmeci, T. Reichert, A. S. Botvina, and M. Bleicher, Nucleosynthesis of light nuclei and hypernuclei in central Au + Au collisions at $\sqrt{s_{NN}} = 3$ GeV, Phys. Rev. C **108**, 054904 (2023).
[51] P. Batyuk, D. Blaschke, M. Bleicher, Y. B. Ivanov, I. Karpenko, S. Merts, M. Nahrgang, H. Petersen, and O. Rogachevsky, Event simulation based on three-fluid hydrodynamics for collisions at energies available at the dubna nuclotron-based ion collider facility and at the facility for antiproton and ion research in darmstadt, Phys. Rev. C **94**, 044917 (2016).
[52] P. Batyuk, D. Blaschke, M. Bleicher, Y. B. Ivanov, I. Karpenko, L. Malinina, S. Merts, M. Nahrgang, H. Petersen, and O. Rogachevsky, Three-fluid hydrodynamics-based event simulator extended by UrQMD final state interactions (THESEUS) for FAIR-NICA-SPSBES/RHIC energies, EPJ Web Conf. **182**, 02056 (2018).
[53] Y. B. Ivanov, Alternative scenarios of relativistic heavy-ion collisions: I. Baryon stopping, Phys. Rev. C **87**, 064904 (2013).
[54] Y. B. Ivanov and A. A. Soldatov, Light fragment production at CERN super proton synchrotron, Eur. Phys. J. A **53**, 218 (2017).
[55] https://www.nndc.bnl.gov/nudat2/getdataset.jsp?nucleus=4HE&unc=nds.
[56] I. N. Mishustin, V. N. Russkikh, and L. M. Satarov, Fluid dynamical model of relativistic heavy ion collision, Sov. J. Nucl. Phys. **54**, 260 (1991).
[57] A. S. Khvorostukin, V. V. Skokov, V. D. Toneev, and K. Redlich, Lattice QCD constraints on the nuclear equation of state, Eur. Phys. J. C **48**, 531 (2006).
[58] V. N. Russkikh and Y. B. Ivanov, Dynamical freeze-out in three-fluid hydrodynamics, Phys. Rev. C **76**, 054907 (2007).
[59] Yu. B. Ivanov and V. N. Russkikh, On freeze-out problem in relativistic hydrodynamics, Phys. At. Nucl. **72**, 1238 (2009).
[60] Y. B. Ivanov and A. A. Soldatov, Correlation between global polarization, angular momentum, and flow in heavy-ion collisions, Phys. Rev. C **102**, 024916 (2020).
[61] W. Reisdorf *et al.* (FOPI Collaboration), Systematics of central heavy ion collisions in the 1*A* GeV regime, Nucl. Phys. A **848**, 366 (2010).
[62] S. Typel, G. Ropke, T. Klahn, D. Blaschke, and H. H. Wolter, Composition and thermodynamics of nuclear matter with light clusters, Phys. Rev. C **81**, 015803 (2010).
[63] P. Danielewicz and Q. B. Pan, Blast of light fragments from central heavy-ion collisions, Phys. Rev. C **46**, 2002 (1992).
[64] C. Kuhrts, M. Beyer, P. Danielewicz, and G. Ropke, Medium corrections in the formation of light charged particles in heavy ion reactions, Phys. Rev. C **63**, 034605 (2001).
[65] A. Ono, Cluster production within antisymmetrized molecular dynamics, EPJ Web Conf. **122**, 11001 (2016).
[66] N. U. Bastian, P. Batyuk, D. Blaschke, P. Danielewicz, Y. B. Ivanov, I. Karpenko, G. Röpke, O. Rogachevsky, and H. H. Wolter, Light cluster production at NICA, Eur. Phys. J. A **52**, 244 (2016).
[67] G. Röpke, D. Blaschke, Y. B. Ivanov, I. Karpenko, O. V. Rogachevsky, and H. H. Wolter, Medium effects on freeze-out of light clusters at NICA energies, Phys. Part. Nucl. Lett. **15**, 225 (2018).
[68] G. Röpke, N. U. Bastian, D. Blaschke, T. Klahn, S. Typel, and H. H. Wolter, Cluster virial expansion for nuclear matter within a quasiparticle statistical approach, Nucl. Phys. A **897**, 70 (2013).
[69] G. Röpke, Nuclear matter equation of state including two-, three-, and four-nucleon correlations, Phys. Rev. C **92**, 054001 (2015).
[70] D. Blaschke, G. Röpke, Y. Ivanov, M. Kozhevnikova, and S. Liebing, Strangeness and light fragment production at high baryon density, Springer Proc. Phys. **250**, 183 (2020).
[71] D. Blaschke, A. V. Friesen, Y. B. Ivanov, Y. L. Kalinovsky, M. Kozhevnikova, S. Liebing, A. Radzhabov, and G. Röpke, QCD phase diagram at NICA Energies: K^+/π^+ horn effect and light clusters in THESEUS, Acta Phys. Pol. B: Proc. Suppl. **14**, 485 (2021).
[72] M. S. Abdallah *et al.* (STAR Collaboration), Disappearance of partonic collectivity in $\sqrt{s_{NN}} = 3$ GeV Au + Au collisions at RHIC, Phys. Lett. B **827**, 137003 (2022).
[73] P. Danielewicz, R. Lacey, and W. G. Lynch, Determination of the equation of state of dense matter, Science **298**, 1592 (2002).
[74] H. Sorge, Elliptical flow: A signature for early pressure in ultrarelativistic nucleus-nucleus collisions, Phys. Rev. Lett. **78**, 2309 (1997).
[75] P. Danielewicz, R. A. Lacey, P. B. Gossiaux, C. Pinkenburg, P. Chung, J. M. Alexander, and R. L. McGrath, Disappearance of elliptic flow: A new probe for the nuclear equation of state, Phys. Rev. Lett. **81**, 2438 (1998).
[76] Y. B. Ivanov and A. A. Soldatov, Elliptic flow in heavy-ion collisions at energies $\sqrt{s_{NN}} = 2.7 - 39$ GeV, Phys. Rev. C **91**, 024914 (2015).
[77] J. Cimerman, I. Karpenko, B. Tomasik, and P. Huovinen, Next-generation multifluid hydrodynamic model for nuclear collisions at $\sqrt{s_{NN}}$ from a few GeV to a hundred GeV, Phys. Rev. C **107**, 044902 (2023).
[78] http://ckp.nrcki.ru/.
[79] http://hlit.jinr.ru/supercomputer_govorun/.